

MIT Open Access Articles

Stretchable Hydrogel Electronics and Devices

The MIT Faculty has made this article openly available. **Please share** how this access benefits you. Your story matters.

Citation: Lin, Shaoting, Hyunwoo Yuk, Teng Zhang, German Alberto Parada, Hyunwoo Koo, Cunjiang Yu, and Xuanhe Zhao. "Stretchable Hydrogel Electronics and Devices." *Advanced Materials* (December 2015): n/a–n/a.

As Published: <http://dx.doi.org/10.1002/adma.201504152>

Publisher: Wiley Blackwell

Persistent URL: <http://hdl.handle.net/1721.1/100280>

Version: Author's final manuscript: final author's manuscript post peer review, without publisher's formatting or copy editing

Terms of use: Creative Commons Attribution-Noncommercial-Share Alike



Advanced Materials

Stretchable, Robust and Biocompatible Hydrogel Electronics and Devices

--Manuscript Draft--

Manuscript Number:	
Full Title:	Stretchable, Robust and Biocompatible Hydrogel Electronics and Devices
Article Type:	Invited Communication
Section/Category:	By Invitation Only: Flexible and Stretchable Devices Special Issue
Keywords:	hydrogel stretchable electronics and devices drug delivery wearable devices biointegrated electronics
Corresponding Author:	Xuanhe Zhao Massachusetts Institute of Technology Cambridge, MA UNITED STATES
Additional Information:	
Question	Response
Please submit a plain text version of your cover letter here. If you are submitting a revision of your manuscript, please do not overwrite your original cover letter. There is an opportunity for you to provide your responses to the reviewers later; please do not add them here.	N/A
Corresponding Author Secondary Information:	
Corresponding Author's Institution:	Massachusetts Institute of Technology
Corresponding Author's Secondary Institution:	
First Author:	Xuanhe Zhao
First Author Secondary Information:	
Order of Authors:	Xuanhe Zhao
Order of Authors Secondary Information:	
Abstract:	Human bodies are mainly composed of hydrogels — polymer networks infiltrated with water. As unprecedented amounts of electronic devices are being integrated with human body, hydrogels with similar physiological and mechanical properties as human tissues represent ideal matrix/coating materials for electronics and devices to achieve long-term effective bio-integrations. However, owing to the weak and brittle nature of common synthetic hydrogels, existing hydrogel electronics and devices mostly suffer from the limitation of low mechanical robustness and low stretchability. Here we report a set of new materials and methods to integrate stretchable conductors, rigid electronic components, and drug-delivery channels and reservoirs into biocompatible and tough hydrogel matrices that contain significant amounts of water (e.g., 70 ~ 95 wt %). As a result, we presented the world's first set of hydrogel-based electronics and devices that are mechanically robust, highly stretchable, biocompatible, and capable of multiple novel functions such as soft, wet and stretchable LED arrays and hydrogel-based sensor-controlled drug-delivery system. We show that the design of robust hydrogel-solid interfaces is particularly important to the functionality and reliability of stretchable hydrogel electronics and devices.

DOI: 10.1002/((please add manuscript number))

Article type: Communication

Stretchable, Robust and Biocompatible Hydrogel Electronics and Devices

Shaoting Lin^{1a}, Hyunwoo Yuk^{1a}, Teng Zhang^{1a}, Hyunwoo Koo^{1,2}, Cunjiang Yu³, and Xuanhe Zhao^{1,4}*

¹ *Soft Active Materials Laboratory, Department of Mechanical Engineering, Massachusetts Institute of Technology, Cambridge, MA 02139, USA;* ² *Samsung Display, Asan-City, Chungcheongnam-Do, Korea*
³ *Department of Mechanical Engineering, University of Houston, Houston, TX 77204, USA;* ⁴ *Department of Civil and Environmental Engineering, Massachusetts Institute of Technology, Cambridge, MA 02139, USA*

^a These authors contribute equally to the current work.

* To whom correspondence should be addressed. Email: zhaox@mit.edu

Animal bodies are mainly composed of hydrogels — polymer networks infiltrated with water. Most biological hydrogels are mechanically flexible yet robust, and they accommodate transportations (e.g., convection and diffusion) and reactions of various essential substances for life – endowing living bodies with exquisite functions such as sensing and responding, self-healing, self-reinforcing and self-regulating et al. To harness hydrogels' unique properties and functions, intensive efforts have been devoted to developing various biomimetic structures and devices based on hydrogels. Examples include hydrogel valves for flow control in microfluidics ^[1], adaptive micro lenses activated by stimuli-responsive hydrogels ^[2], color-tunable colloidal crystals from hydrogel particles ^[3, 4], complex micro patterns switched by hydrogel-actuated nanostructures ^[5], responsive buckled hydrogel surfaces^[6], and gripping and self-walking structures based on hydrogels ^[7-9]. In particular, as unprecedented amounts of electronic devices are being integrated with human body ^[10-14], hydrogels with similar physiological and mechanical properties as human

1
2
3
4
5 tissues represent ideal matrix/coating materials for electronics and devices to achieve long-term
6
7 effective bio-integrations ^[15-17]. However, owing to the weak and brittle nature of common
8
9 synthetic hydrogels, existing hydrogel electronics and devices mostly suffer from the limitation of
10
11 low mechanical robustness and low stretchability. On the other hand, while hydrogels with
12
13 extraordinary mechanical properties, or so-called tough hydrogels, have been recently developed
14
15 ^[18-22], it is still challenging to fabricate tough hydrogels into stretchable electronics and devices
16
17
18 capable of novel functions. The design of robust, stretchable and biocompatible hydrogel
19
20 electronics and devices represents a critical challenge in the emerging field of soft materials,
21
22 electronics and devices.
23
24
25

26
27 Here we report a set of new materials and methods to integrate stretchable conductors, rigid
28
29 electronic components, and drug-delivery channels and reservoirs into biocompatible and tough
30
31 hydrogel matrices that contain significant amounts of water (e.g., 70 ~ 95 wt %). The resultant
32
33 hydrogel-based electronics and devices are mechanically robust, highly stretchable, biocompatible,
34
35 and capable of multiple novel functions. We show that the design of robust hydrogel-solid
36
37 interfaces is particularly important to the functionality and reliability of stretchable hydrogel
38
39 electronics and devices. Programmable delivery and sustained release of drugs can be achieved by
40
41 controlling the flow of drug solutions through selected channels and reservoirs in hydrogel
42
43 matrices at both undeformed and highly stretched states. We further demonstrate novel
44
45 applications including a stretchable LED array encapsulated in biocompatible hydrogel matrix,
46
47 and a smart hydrogel wound dresser that is highly stretchable, transparent, and capable of sensing
48
49 temperatures at different locations on the skin and sustained release of various drugs to specific
50
51 locations accordingly.
52
53
54
55
56
57
58
59
60
61
62
63
64
65

Figure 1 gives a generic illustration of the design of stretchable hydrogel electronics and devices. A biocompatible, highly stretchable and robust hydrogel provide a soft and wet matrix for electronics and devices – drastically different from dry elastomer/polymer matrices for conventional stretchable electronics. Functional electronic components such as conductors, microchips, transducers, resistors, capacitors are embedded inside or attached on the surface of the hydrogel (**Fig. 1a**). The electronic components may be covered (or partially covered) by an insulating layer such as polydimethylsiloxane (PDMS) to maintain their normal functions in wet environments of hydrogels. Drug-delivery channels and reservoirs are further patterned in the hydrogel matrix, such that when drug solutions flow through the channels and/or into the reservoirs, they can diffuse out of the hydrogel to give programmable and sustained release of drugs (**Fig. 1a**). As the hydrogel electronic device is stretched, flexible electronic components can deform together with the device but rigid components will maintain their undeformed shapes, which requires larger deformation of hydrogel around rigid components than others (**Fig. 1b**). Therefore, in order to maintain reliability and functionality of the device, the hydrogel matrix and the interfaces between hydrogel and functional components need to be tough and robust under large deformation.

The design of tough hydrogels relies on a combination of long-chain polymer networks that are highly stretchable and other components (such as other polymer networks) that can dissipate significant mechanical energy under deformation ^[23-25]. In **Table 1**, we provide a set of polymer candidates for the long-chain networks including Polyacrylamide (PAAm) and Polyethylene glycol (PEG) that are covalently crosslinked by N,N-Methylenebisacrylamide (BIS) and Diacrylate (DA) respectively, and the dissipative networks including alginate, hyaluronan and chitosan that are reversibly crosslinked by calcium sulfate, iron (III) chloride, sodium tripolyphosphate respectively. **Table 1** further gives the optimal concentrations for each

1
2
3
4
5 combination of networks and crosslinkers that can lead to tough hydrogels [26-28]. The
6
7 biocompatibility has been validated for hydrogels with individual polymer network of PAAm,
8
9 PEG, alginate, hyaluronan or chitosan [29], as well as for PAAm-alginate and PEG-alginate tough
10
11 hydrogels [27, 30]. Since the biocompatible PAAm-alginate hydrogel gives the highest stretchability
12
13 (~ 21 times) and fracture toughness (~ 9,000 Jm⁻²) among all candidates in **Table 1**, we choose
14
15 PAAm-alginate as the hydrogel matrix for stretchable electronics and devices in the current study.
16
17 It should be noted that using other tough hydrogels in **Table 1** as matrices may have other benefits
18
19 in applications; for example, the PEG-alginate and PEG-hyaluronan hydrogel matrices can allow
20
21 encapsulation of viable cells in hydrogel electronics and devices [27, 31].
22
23
24
25
26

27
28 Now that a stretchable and robust hydrogel matrix has been determined, we will discuss
29
30 methods to integrate various functional components including conductive wires, rigid chips, and
31
32 drug-delivery channels and reservoirs into the hydrogel matrix. Given the high mechanical
33
34 robustness and biocompatibility of titanium, we choose titanium wires (Unkamen Supplies,
35
36 Diameters D : 0.08 mm ~ 0.2 mm) as the candidate for conductive components in hydrogel
37
38 electronics and devices. **Figure S2** illustrates the procedure to encapsulate titanium wires into
39
40 hydrogel matrix to form transparent, stretchable and robust hydrogel conductors. In brief, the
41
42 surface of titanium wire was functionalized with silane 3-(Trimethoxysilyl) Propyl Methacrylate
43
44 (TMSPMA) (See experimental section for details on silane functionalization.) The titanium wire
45
46 was then deformed into a sinusoidal shape with amplitude A and wavelength L (**Fig. 2a**), either
47
48 through the constraint of a mold (for relatively thin wires, e.g. diameter 0.08 mm) or plastic
49
50 deformation (for relatively thick wires, e.g. diameter 0.2 mm) [11, 32-35]. Thereafter, pre-gel solution
51
52 was casted around the deformed titanium wire and cured in a mold that determines the shape and
53
54 dimensions of the hydrogel matrix. During the curing process, the PAAm long-chain network in
55
56
57
58
59
60
61
62
63
64
65

1
2
3
4
5 the hydrogel was covalently anchored on the titanium wire (**Fig. S1**), giving extremely tough
6
7 interface between hydrogel matrix and conductive wire (i.e., interfacial toughness over 1500 Jm⁻
8
9 2) [28]. **Figure 2b** demonstrates a hydrogel conductor with $A/L=0.23$ for the encapsulated titanium
10
11 wire. It can be seen that, except for the region of the wire, the hydrogel conductor is transparent –
12
13 clearly showing the background of a white paper. As the hydrogel conductor is deformed to
14
15 different stretches λ (defined as deformed length over undeformed length), the sinusoidal-shaped
16
17 wire decreases its amplitude and increases its wavelength, enabling high stretchability of the
18
19 hydrogel conductor (**Fig. 2b**). Because the hydrogel is much more compliant than titanium wire
20
21 (shear modulus 10 kPa vs. 40 GPa) and highly stretchable, it can accommodate the shape change
22
23 of the titanium wire without fracture or delamination (**Fig. 2b**). Finite-element model (using
24
25 software, ABAQUS) of the hydrogel conductor indicates that the maximum principle strain in
26
27 hydrogel matrix occurs around stationary points of the wavy interface between hydrogel and
28
29 titanium wire (**Fig. 2b**) (See supplementary material for details of the finite-element model). Once
30
31 the titanium wire becomes fully straight, the hydrogel conductor cannot be further stretched
32
33 without inducing plastic deformation or failure of the wire^[36] (See **Fig. S4**). Therefore, the
34
35 theoretical limit of the stretch on the hydrogel conductor can be calculated as
36
37
38
39
40
41
42
43

$$\lambda_{\max} = \frac{1}{L} \int_0^L \sqrt{1 + \frac{4A^2\pi^2}{L^2} \cos^2\left(\frac{x}{L} \cdot 2\pi\right)} dx \quad (1)$$

44
45
46
47
48
49 In **Fig. 2c**, we plot the calculated λ_{\max} as a function of A/L , and compare the theoretical
50
51 limit with the maximum stretches measured in hydrogel conductors that contain titanium wires
52
53 with and without silanized surfaces. Since the silanized titanium has a robust interface with the
54
55 tough hydrogel matrix^[28], the corresponding hydrogel conductor can reach very high maximum
56
57 stretches (e.g., >2), only slightly lower than the theoretical limits (**Fig. 2c**). For example, **Video**
58
59
60
61
62
63
64
65

1
2
3
4
5 **S1** demonstrates a hydrogel conductor that contains a silanized titanium wire ($A/L=0.32$) being
6 stretched to the theoretical limit of stretch $\lambda_{\text{max}} \approx 1.58$. On the other hand, the hydrogel conductor
7 with pristine titanium wire fails quickly under moderate stretch (**Fig. S3**), due to the debonding
8 between titanium wire and hydrogel matrix. Therefore, the measured maximum stretch for
9 hydrogel conductor with pristine titanium wire is much lower than the value of silanized wire with
10 the same A/L and the theoretical limit (**Fig. 2c**). These results prove that robust hydrogel-
11 conductive-wire interfaces are critical to the reliability of stretchable hydrogel conductors. In
12 addition, as shown on **Fig. 2d**, the hydrogel conductor can sustain multiple cycles (i.e., 10,000) of
13 high stretch (i.e., 3), while maintaining constant resistance. While hydrogels that contain high
14 concentrations of salt solutions have been used as transparent ionic conductors^[37, 38], the current
15 work presents a simple method to fabricate transparent, highly stretchable and robust electronic
16 conductors based on biocompatible hydrogels.
17
18
19
20
21
22
23
24
25
26
27
28
29
30
31
32
33
34

35 We next discuss the method to integrate relatively rigid components such as rigid chips
36 into the hydrogel matrix. We will use chips made of PDMS (DowCorning Sylgard 184 Silicone
37 Elastomer Kit) to represent the rigid electronic components, since these electronic components are
38 likely to be covered by PDMS for insulation from wet environment of the hydrogel matrix. **Figure**
39 **S5** illustrates the procedure to attach rigid electronic components on the surface of (or embed them
40 inside) hydrogel matrix. Since it is challenging to form tough interface between hydrogels and
41 PDMS^[39], we used glass slides as intermediate layers to form tough bonding between chips and
42 hydrogel matrix. One side of the glass slide and the PDMS chip were exposed to oxygen plasma
43 for 2 min, and physically contacted each other right after plasma treatment to form siloxane
44 covalent linkage between the glass slide and PDMS chip. Thereafter, the exposed surface of the
45 attached glass slide was again exposed to oxygen plasma for 5 min and covered by TMSPMA
46
47
48
49
50
51
52
53
54
55
56
57
58
59
60
61
62
63
64
65

aqueous solution for 2 hours. To adhere the PDMS chips on the surface of hydrogel matrix, we fabricated acrylic mold with laser-cut holes to host the PDMS-glass assemblies. Each assembly was put into a hole in the mold with functionalized glass side up, and then the pre-gel solution was poured into the mold. During the curing process, the PAAm long-chain network in the hydrogel was covalently anchored on glass slide, which gives high interfacial toughness over 1500 Jm^{-2} (**Fig. 3a**)^[28]. **Figure 3b** and **Video S2** demonstrates a PDMS chip bonded on the surface of hydrogel using silanized glass slide. It can be seen that the chip does not detach from the hydrogel, even when it is pulled by a tweezer that significantly deforms the hydrogel matrix. On the other hand, if the chip with pristine glass is physically attached on hydrogel, it can be easily detached by the tweezer, indicating the importance of functionalized and robust interfaces in hydrogel electronics (**Fig. 3c**).

To predict whether a chip will debond from hydrogel matrix under deformation, we develop a plane-strain island-substrate model using finite-element software, ABAQUS^[40]. (See supplementary material for details of the finite-element model.) The energy release rate G for initiating interfacial cracks between the chip and hydrogel substrate can be expressed as

$$\frac{G}{\mu L} = f\left(\lambda, \frac{S}{L}, \frac{H}{L}\right) \quad (2)$$

where μ is the shear modulus of the hydrogel modeled as a neo-Hookean material, L the width of the chip, λ the applied stretch, S center-to-center distance between two adjacent chips, H thickness of undeformed hydrogel substrate, and $f(\bullet)$ a non-dimensional function. Since $G/\mu L$ is a monotonic increasing function of H/L (**Fig. S7**), we focus on the case with infinitely deep substrate (i.e., $H/L = \infty$) to be conservative in the design. The calculated $G/\mu L$ from the finite-element model is plotted in **Fig. 3d** as functions of λ and S/L . The typical values of interfacial

1
2
3
4
5 toughness between chips and hydrogels with and without silanized interfaces are also given in **Fig.**
6
7 **3d** for comparison. When the energy release rate reaches the interfacial toughness, cracks initiate
8
9 on the interface inducing failure of the hydrogel device. The model shows that the chip-hydrogel
10
11 structure with silanized interface can sustain very high stretch without debonding, but the structure
12
13 without silanized interface will debond at relative low stretch (e.g., $\lambda = 1.5$). **Figure 3e** further
14
15 demonstrate that the chip bonded with silanized interface does not detach from hydrogel matrix
16
17 under high stretch (e.g., $\lambda = 3$). Since the hydrogel is soft, wet and biocompatible, a sheet of
18
19 hydrogel (thickness ~ 1.5 mm) with multiple patterned chips can conformably attach to different
20
21 regions of human body (e.g., the elbow in **Fig. 3f**). Movement of the body part deforms the
22
23 hydrogel but will not debond the chips.
24
25
26
27
28

29
30 In addition to bonding on hydrogel surfaces, the rigid chips can also be encapsulated inside
31
32 hydrogel matrices. In this case, tough interfaces between the chips and hydrogel can be achieved
33
34 via multiple intermediate glass slides (**Fig. S5**). For example, **Figure 3g** and **Video S3** illustrate
35
36 a hydrogel electronic device that encapsulates an array of LED lights connected by stretchable
37
38 wires (See **Fig. S8** for details on fabrication). This new design of hydrogel-encapsulated LED array
39
40 is soft, biocompatible, transparent, and robust under large deformations such as high stretch (**Fig.**
41
42 **3g**) and conformal deformation on human body (**Video S3**).
43
44
45

46
47 One unique advantage of hydrogels over dry polymers as matrices for stretchable
48
49 electronics and devices is the capability of drug diffusion in hydrogels^[41, 42]. In the current design,
50
51 we pattern drug-delivery channels and reservoirs in the hydrogel matrix. Drug solutions can be fed
52
53 to the channels and reservoirs from external sources via controlled convections (**Fig. 4a**). If the
54
55 hydrogel matrix is in contact with human body, the drug solutions can diffuse from the channels
56
57 and reservoirs out of the hydrogel matrix and maintain a sustained release at controlled locations
58
59
60
61
62
63
64
65

in/on the body. **Fig. 4b** demonstrates the diffusion of a mock drug, 2% aqueous solution of a red food dye (McCormick), from a drug-release channel in a hydrogel matrix over time (See **Table S1** for detailed ingredients of the mock drug). To simplify the analysis, we set the diameter of the drug-delivery channel close to the thickness of the hydrogel sheet, and seal the hydrogel sheet with silicone oil. This leads to approximately one-dimensional diffusion of the drug solution in the hydrogel sheet governed by

$$\frac{\partial C(t, y)}{\partial t} = D \frac{\partial^2 C(t, y)}{\partial y^2} \quad (3)$$

where C is the concentration of the drug at a point in the hydrogel, t the current time, y vertical position of the point in hydrogel at deformed state, and D the diffusion coefficient of the drug in the hydrogel. Since drug concentration on the wall of the channel (i.e., $y = 0$) is fixed to be C_0 over time, Eq. (3) can be solved as

$$\frac{C(t, y)}{C_0} = 1 - \operatorname{erf}\left(\frac{y}{2\sqrt{Dt}}\right) \quad (4)$$

where $\operatorname{erf}(\bullet)$ is the error function. We plot the measured values of C/C_0 at different times and different locations in the hydrogel as functions of y/\sqrt{t} in **Fig. 4d**, and fit the diffusion coefficient of the drug in the hydrogel to be $1.5 \times 10^{-10} \text{ m}^2/\text{s}$. In addition, when the hydrogel sheet is stretched (e.g., $\lambda = 1.6$ in **Fig. 4c**), it still accommodates drug diffusion without burst leakage, owing to the high toughness and stretchability of the hydrogel. The drug diffusion coefficient in the stretched hydrogel (**Fig. 4e**) is $3 \times 10^{-10} \text{ m}^2/\text{s}$, higher than that in undeformed hydrogel, possibly due to the increase of mesh size in stretched hydrogel. In **Fig. 4f**, we further demonstrate that multiple drugs represented by different food dyes (See **Table S1** for detailed

1
2
3
4
5 ingredients) with different colors can be released simultaneously in the hydrogel device under
6
7 multiple cycles of high stretches.
8
9

10 To further demonstrate novel functions of stretchable and biocompatible hydrogel
11 electronics and devices, we fabricate a smart wound dressing that combines temperature sensors,
12 drug delivery channels and reservoirs patterned into a stretchable and transparent tough hydrogel
13 sheet (**Fig. 5**). **Figure S9** illustrates the procedure to pattern temperature sensors (24PetWatch),
14 non-diffusive drug-delivery channels (made of plastic tubes), and diffusive drug reservoirs in the
15 hydrogel matrix. (See experimental methods for details of the procedure.) As illustrated in **Fig. 5a**,
16 the temperature sensors were patterned into a 3 by 3 matrix with a drug-delivery reservoir next to
17 each sensor. The smart wound dressing can give programmable and sustained deliveries of
18 different drugs at various locations over human skin according to the temperatures measured at
19 those locations (**Fig. 5**). For example, as a sensor detects that the temperature at a location increases
20 above a threshold (e.g., 35°C) at a certain time, a drug solution can be delivered through the non-
21 diffusive drug-delivery channel to the corresponding drug reservoir and then diffuse out of the
22 hydrogel matrix in a controlled and sustained manner (**Fig. 5a**). The same procedure can be
23 repeated according to the measurements from different temperature sensors over time (**Fig. 5a-c**).
24 **Figure 5c-f** and **Video S4** illustrates the controlled delivery and sustained releases of various drugs
25 at different locations according to the temperatures measured at different times.
26
27
28
29
30
31
32
33
34
35
36
37
38
39
40
41
42
43
44
45
46
47
48
49

50 In summary, we report a set of novel materials and methods to integrate various
51 electronic components and drug-delivery channels and reservoirs into tough hydrogel matrix —
52 achieving stretchable, robust and biocompatible hydrogel electronics and devices. The
53 compliant hydrogel matrix can accommodate both deformable (e.g., wavy wires and channels)
54 and rigid (e.g., silicon chips) components embedded in or attached on it, even when the hydrogel
55
56
57
58
59
60
61
62
63
64
65

1
2
3
4
5 electronics and devices are highly deformed. Experiments and numerical simulation show that
6
7 the interfaces between hydrogel matrix and functional components are often subjected to high
8
9 stresses, due to the mechanical mismatch. Surface functionalization (e.g., coating and
10
11 silanization) of the functional components can give tough covalent bonding to the hydrogel,
12
13 which is critical to functionality and reliability of hydrogel electronics and devices. We further
14
15 demonstrate novel applications of hydrogel electronics and devices including a soft, wet,
16
17 transparent and stretchable LED array, and a smart wound dresser capable of sensing
18
19 temperatures of various locations on the skin, delivering different drugs to these locations, and
20
21 subsequently maintaining sustained releases of drugs.
22
23
24
25
26
27
28
29

30 **Experimental Methods**

31
32
33 *Synthesis of tough hydrogels.* We followed the previous reported protocol for synthesis of
34
35 PAAm-alginate tough hydrogel [43]. A precursor solution was prepared by mixing 4.1 mL 4.8 wt. %
36
37 alginate (Sigma, A2033) and 5.5 mL 18.7 wt. % acrylamide (Sigma, A8887). We added 377 μ L
38
39 0.2 g/100ml N,N-methylenebisacrylamide (Sigma, 146072) as the crosslinker for polyacrylamide
40
41 and 102 μ L 0.2 M ammonium persulphate (Sigma, 248614) as an initiator for polyacrylamide.
42
43 After degassing the precursor solution in a vacuum chamber, we added 200 μ L 1 M calcium
44
45 sulphate (Sigma, C3771) as the ionic crosslinker for alginate and 8.2 μ L N,N,N',N'-
46
47 tetramethylethylenediamine (Sigma, T7024-50M) as the crosslinking accelerator for acrylamide.
48
49 Thereafter, the precursor solution was poured into an acrylic mold and was subjected to ultraviolet
50
51 light for 60 minutes with 8 W power and 254 nm wavelength to cure the hydrogel.
52
53
54
55
56
57
58
59
60
61
62
63
64
65

1
2
3
4
5
6
7
8
9
10
11
12
13
14
15
16
17
18
19
20
21
22
23
24
25
26
27
28
29
30
31
32
33
34
35
36
37
38
39
40
41
42

The PAAm-hyaluronic acid tough hydrogel was synthesized by mixing 10 mL of degassed precursor solution (18 wt. % AAm, 2 wt. % HA, 0.026 wt. % MBAA and 0.06 wt. % APS) with 60 μ L of iron (III) chloride solution (0.05 M) and TEMED (0.0025 the weight of AAm). The PAAm-chitosan tough hydrogel was synthesized by mixing 10 mL of degassed precursor solution (24 wt. % AAm, 2 wt. % chitosan, 1 wt. % acetic acid, 0.034 wt. % MBAA and 0.084 wt. % APS) with 60 μ L of TPP solution (0.05 M) and TEMED (0.0025 the weight of AAm). The PEGDA-alginate tough hydrogel was synthesized by mixing 10 mL of a degassed precursor solution (20 wt. % PEGDA and 2.5 wt. % sodium alginate) with calcium sulfate slurry (0.068 the weight of sodium alginate) and Irgacure 2959 (0.0018 the weight of PEGDA). The PEGDA-hyaluronan tough hydrogel was synthesized by mixing 10 mL of a degassed precursor solution (20 wt. % PEGDA and 2 wt. % HA) with 60 μ L of iron chloride solution (0.05 M) and Irgacure 2959 (0.0018 the weight of PEGDA). The PEGDA-chitosan tough hydrogel was synthesized by mixing 10 mL of a degassed precursor solution (20 wt. % PEGDA, 2 wt. % chitosan and 1 wt. % acetic acid) with 60 μ L of TPP (0.05 M) and Irgacure 2959 (0.0018 the weight of PEGDA). The curing procedure was identical to the PAAm-alginate tough hydrogel.

43
44
45
46
47
48
49
50
51
52
53
54
55
56
57
58
59
60
61
62
63
64
65

Silanization and grafting of glass slide and titanium wire. The surfaces of glass and titanium were functionalized by grafting functional silane TMSPMA. Solid substrates were thoroughly cleaned with acetone, ethanol and deionized water in order, and completely dried before the next step. Cleaned substrates were treated by oxygen plasma (30 W with 200 mTorr pressure, Harrick Plasma PDC-001) for 5 min. Right after the plasma treatment, substrate surface was covered with 5 mL of the silane solution (100 mL deionized water, 10 μ L of acetic acid with pH 3.5 and 2 wt. % of TMSPMA) and incubated for 2 hours in the room temperature. Substrates were

1
2
3
4
5 washed with ethanol and completely dried. Functionalized substrates were stored in low humidity
6
7 condition before used for experiments.
8
9

10
11 During oxygen plasma treatment of the solids, oxide layers on the surfaces of the solids
12
13 (silicon oxide on glass and titanium oxide on titanium) were reacted into hydrophilic hydroxyl
14
15 groups by oxygen radicals produced by oxygen plasma. These hydroxyl groups on the oxide layer
16
17 can readily form hydrogen bonds with silanes in the functionalization solution generating a self-
18
19 assembled layer of silanes on the oxide layers ^[44]. Notably, methyl groups in TMSPMA are readily
20
21 hydroxylated in acidic aqueous environment and form silanes. These hydrogen bonds between
22
23 surface oxides and silanes become chemically stable siloxane bonds with removal of water forming
24
25 strongly grafted TMSPMA onto oxide layers on various solids ^[45].
26
27
28
29
30

31
32 Grafted TMSPMA has methacrylate terminal group which can form covalent linkage with
33
34 acrylate groups in acrylamide under radical crosslinking process, generating chemically anchored
35
36 long-chain polymer network onto various solid surfaces ^[46]. Since the long-chain polymer
37
38 networks in hydrogels are chemically anchored onto solid surfaces via strong and stable covalent
39
40 bonds, the interfaces can achieve relatively high intrinsic work of adhesion than physically
41
42 attached hydrogels. The silane functionalization chemistry is summarized in **Fig. S1**.
43
44
45
46

47 *Adhesion between PDMS and glass slide.* PDMS chips were fabricated by mixing resin
48
49 and crosslinker with 10:1 weight ratio (DowCorning Sylgard 184 Silicone Elastomer Kit), and
50
51 cure it for 5 hours at 90 °C. PDMS chips were covalently bonded onto glass slide by introducing
52
53 both surface with oxygen plasma for 2 min and physically contact both surfaces. It is well known
54
55 that oxygen plasma generates hydroxyl groups on both glass and PDMS surface, and these Si-OH
56
57 groups form covalent siloxane bond at their physical contact ^[47].
58
59
60
61
62
63
64
65

1
2
3
4
5
6
7
8
9
10
11
12
13
14
15
16
17
18
19
20
21
22
23
24
25
26
27
28
29
30
31
32
33
34
35
36
37
38
39
40
41
42
43
44
45
46
47
48
49
50
51
52
53
54
55
56
57
58
59
60
61
62
63
64
65

Fabrication of sinusoidal titanium wire. Plastically deformable titanium wire (Unkamen Supplies, Diameters: 0.08 mm ~ 0.2 mm) was formed into wavy shape by squeezing linear wire in between wavy acrylic mold. Since titanium wire is plastically deformable, the amplitude and period of sinusoidal shape were controlled by using different geometry of molds (**Fig. S2a**).

The measurement of stretchability and resistivity of hydrogel with titanium wire encapsulated. The stretchability of the tough hydrogel with titanium wire encapsulated was measured using universal machine (2 kN load cell; Zwick / Roell Z2.5). Before curing the pre-gel solution, sinusoid titanium wire was placed inside the mold measuring 70 mm × 25 mm × 3 mm (**Fig. S2b**). The resultant sample was stretched at 1/min using universal testing machine (**Fig. S2c**), which gives the representative stress-stretch curves as shown in **Fig. S3a**. For the hydrogel with pristine titanium wire encapsulated, the detachment (**Fig. S3b**) between titanium wire and hydrogel occurs, which gives the maximum stretch λ_{max} . While for the hydrogel with silanized titanium wire encapsulated, no detachment can be observed till the titanium wire is stretched to the locking stretch, which gives the maximum stretch λ_{max} . To fully understand the locking stretch of the sample with chemically anchored titanium wire, we calculated the theoretical locking stretch of a sinusoidal titanium wire. One segment in the titanium wire can be expressed as $y = A \sin\left(\frac{x}{L} \cdot 2\pi\right)$ (see **Fig. 2a**). Since the arc length of a curve is $\int_a^b \sqrt{1 + (y')^2} dx$, the theoretical locking stretch of a sinusoidal titanium wire can be expressed as Eq. (1). In addition to the measurement of stretchability, the electrical resistance was measured using the same test set-up by multimeter.

Preparation and operation of smart wound dressing. The smart wound dressing sample was fabricated by making channels and reservoirs using both patterned acrylic mold and sacrificial

1
2
3
4
5
6
7
8
9
10
11
12
13
14
15
16
17
18
19
20
21
22
23
24
25
26
27
28
29
30
31
32
33
34
35
36
37
38
39
40
41
42
43
44
gelatin ^[48]. **Figure S9** shows the schematic illustration of fabrication procedures. A patterned acrylic mold was made using laser cut machine (Epilog Mini/Helix) and thereafter the PAAm-alginate precursor solution was poured into the mold. After the sample was fully cured in UV oven for 60 minutes with 8 W power and 254 nm wavelength, heated gelatin solution (Knox, 10 wt. % at 70 °C) was infused into the shaped reservoirs with the diameter of 8mm and EVA tubings with outside diameter of 1.52 mm and wall thickness of 0.51 mm (McMaster, 1883T1) was placed in the shaped channels. The sample with both gelatin disks and EVA tubings was stored in refrigerator (5 °C) for 5 min. Then the temperature sensors (24PetWatch) were placed beside the reservoirs and the sample was again covered with precursor solution, encapsulated with gelatin disks, EVA tubings and temperature sensors. The whole sample was further cured in room temperature for 30 min. After the second curing, the entire wound dressing was placed at oven (70 °C) for 10 min. Liquefied gelatin was wash away from the tough hydrogel matrix by flowing deionized water multiple times through channels and reservoirs. During the operation of the smart wound dressing, a heat gun was applied to induce concentrated heat to increase local temperature of the wound dressing, and a drug solution was pumped into the corresponding drug reservoir once the temperature at a location increased over the critical value.

45 **Acknowledgement**

46
47
48
49
50
51
52
53
54
55
56
57
58
59
60
61
62
63
64
65
The work was supported by ONR (No. N00014-14-1-0528) and NSF (No. CMMI-1253495). H. K. acknowledges the financial support from Samsung. X. Z. acknowledges the Faculty Award for Shared Experimental Facility from MIT Materials Research Science and Engineering Center. S. L. and X. Z. acknowledge the help from Zhifei Ge and Cullen Buie on diffusion test.

Table 1. Compositions of a set of tough hydrogels with long-chain and dissipative networks

		Dissipative networks		
		Alginate	HA	Chitosan
Long-chain networks	PAAm	12 wt. % AAm, 0.017 wt. % MBAA, 2 wt. % alginate, 200 μ L of CaSO ₄ (1 M) per 10 mL precursor	18 wt. % AAm, 0.026 wt. % MBAA, 2 wt. % HA, 60 μ L of iron (III) chloride (0.05 M) per 10 mL precursor	24 wt. % AAm, 0.034 wt. % MBAA, 2 wt. % chitosan, 60 μ L of TPP (0.05 M) per 10 mL precursor
	PEGDA	20 wt. % PEGDA, 2.5 wt. % alginate, 200 μ L of CaSO ₄ (1 M) per 10 mL precursor	20 wt. % PEGDA, 2 wt. % HA, 60 μ L of iron (III) chloride (0.05 M) per 10 mL precursor	20 wt. % PEGDA, 2 wt. % Chitosan, 60 μ L of TPP (0.05 M) per 10 mL precursor

Figures and Figure Captions

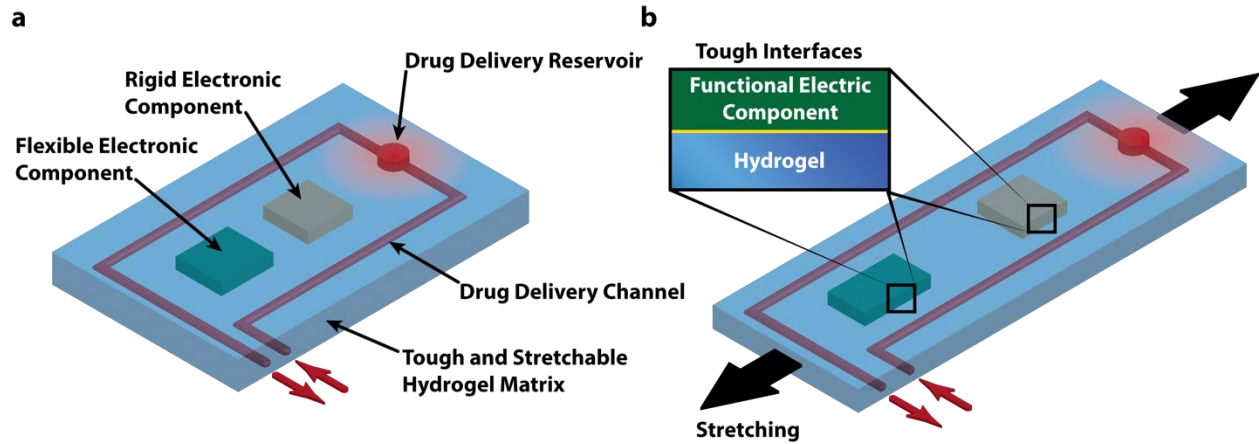
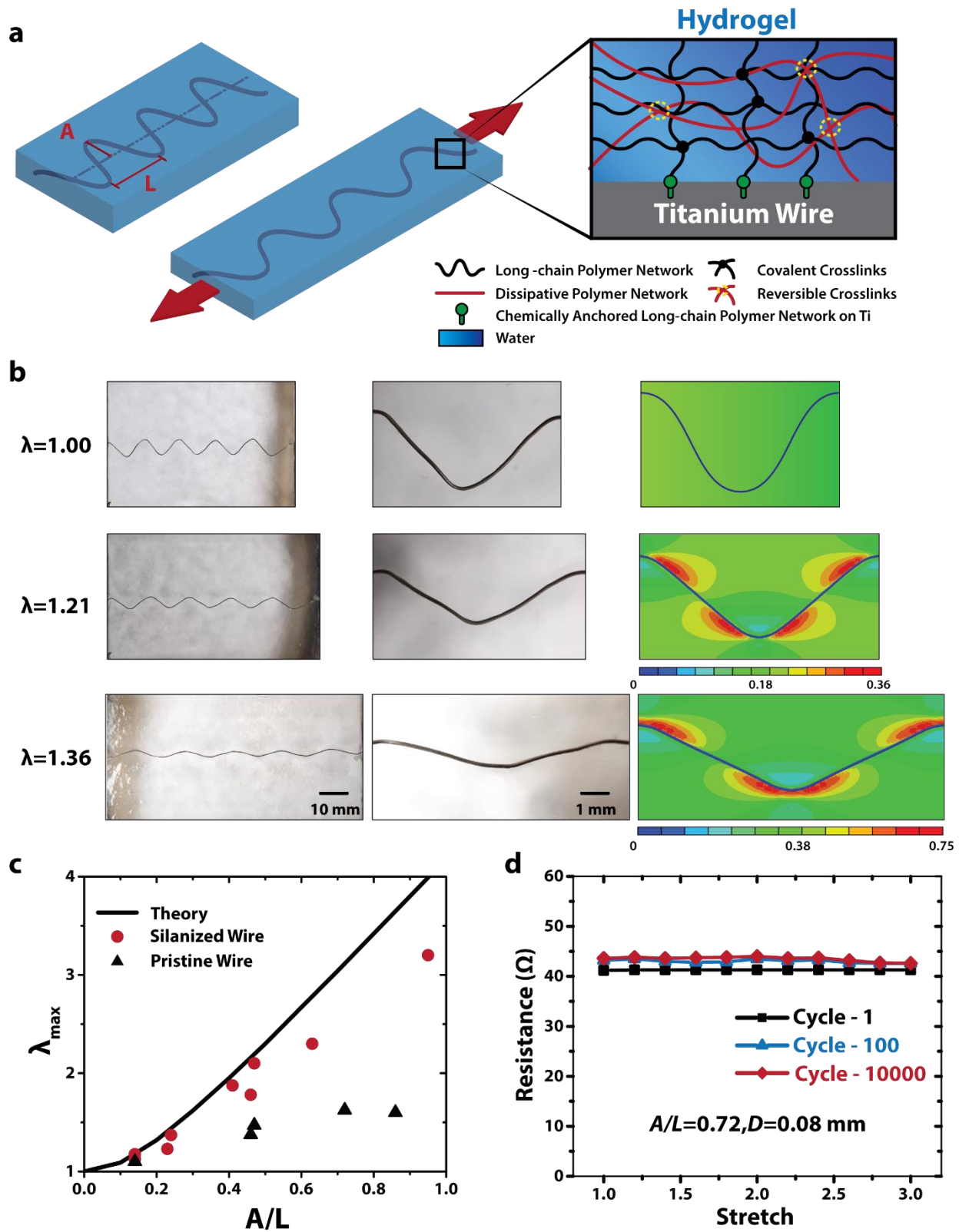
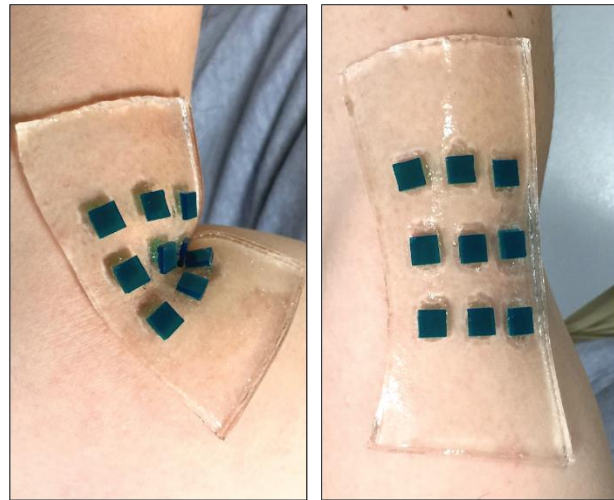
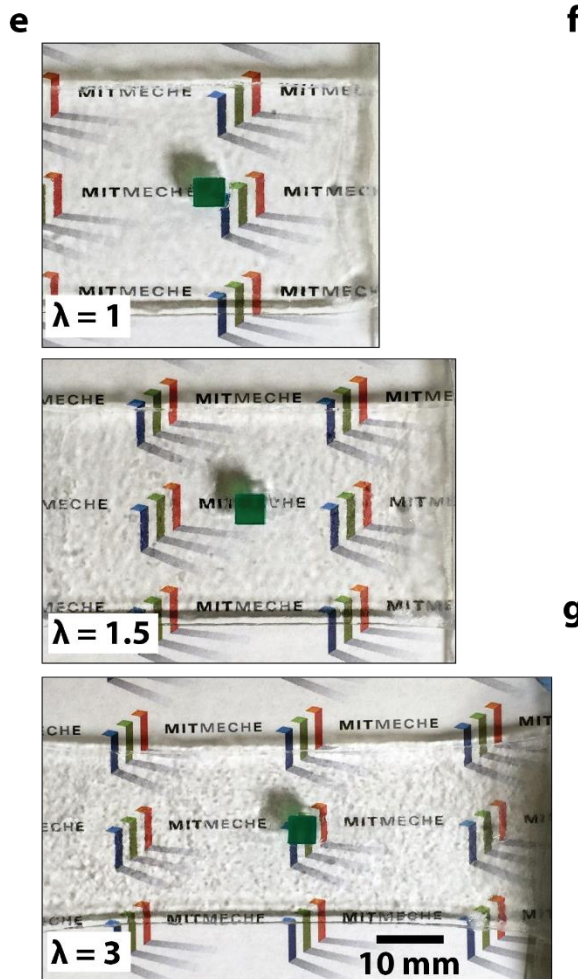
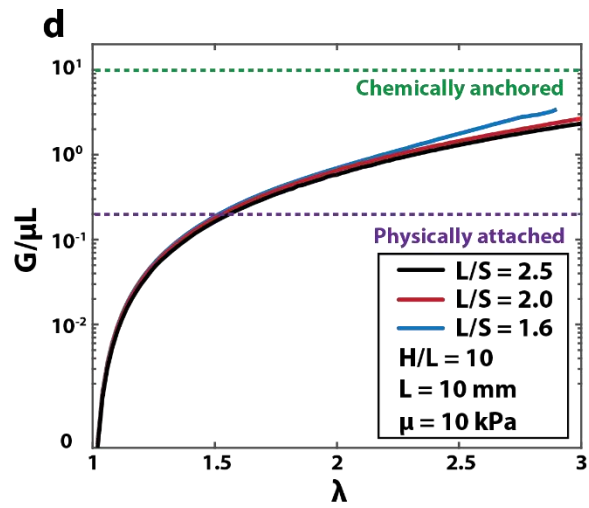
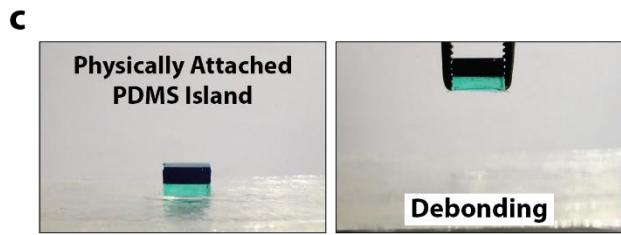
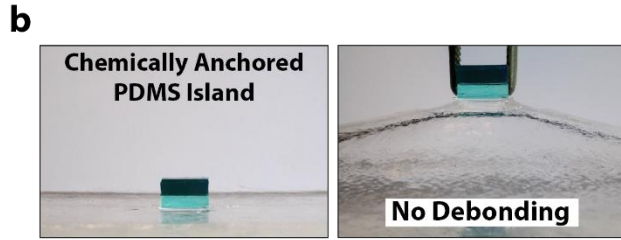
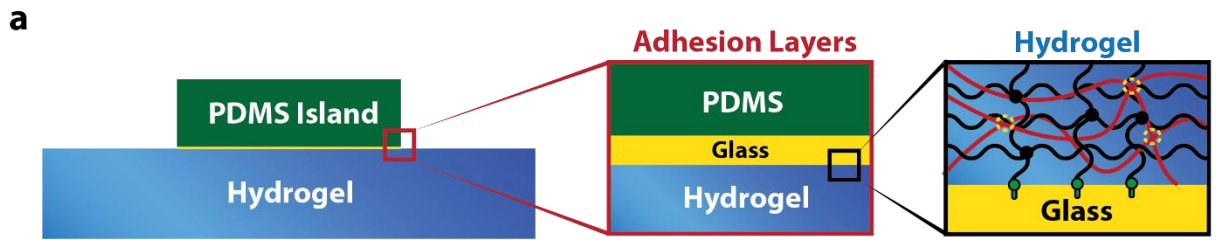


Figure 1. Schematic illustration of the design of stretchable hydrogel electronics and devices.

a) Functional electronic components such as conductors, microchips, transducers, resistors, and capacitors are embedded inside or attached on the surface of the hydrogel. Drug-delivery channels and reservoirs are patterned in the hydrogel matrix, and they can diffuse drugs out of the hydrogel to give programmable and sustained release of drugs. **b)** As the hydrogel electronic device is stretched, flexible electronic components can deform together with the device but rigid components will maintain their undeformed shapes, which requires robust interfaces between electronic components and hydrogel matrix.



1
2
3
4
5
6 **Figure 2. Integration of wavy titanium wires in tough hydrogel matrix.** a) Schematic
7 illustration of the transparent, highly stretchable and robust hydrogel electronic (DC) conductor.
8 Long-chain polymer network of tough hydrogel matrix is chemically anchored onto silanized
9 titanium surface via covalent crosslinks. **b)** The wavy wire can be highly stretched together with
10 hydrogel matrix without fracture or debonding due to robust adhesion between wire and hydrogel
11 matrix. Finite-element simulation shows maximum principal strain of the hydrogel matrix. **c)** The
12 calculated λ_{\max} as a function of A/L in comparison with experimentally measured maximum
13 stretches in hydrogel conductors that contain titanium wires with and without silanized surfaces.
14
15 **d)** The hydrogel conductor ($A/L=0.72$, diameter $D=0.08\text{mm}$) can sustain multiple cycles (i.e.,
16 10,000) of high stretch (i.e., 3), while maintaining constant resistance.
17
18
19
20
21
22
23
24
25
26
27
28
29
30
31
32
33
34
35
36
37
38
39
40
41
42
43
44
45
46
47
48
49
50
51
52
53
54
55
56
57
58
59
60
61
62
63
64
65



1
2
3
4
5 **Figure 3. Integration of rigid chips on the surface of (or inside) tough hydrogel matrix. a)**
6
7 Schematic illustration of a rigid PDMS chip bonded on the surface of hydrogel. Glass slide is used
8
9 to form stable and robust adhesion layer between PDMS chip and tough hydrogel. Oxygen plasma
10
11 treated PDMS and glass slide surface are covalently bonded through siloxane bond, while
12
13 silanization of the glass slide gives tough covalent bonding to hydrogel. **b)** Chemically anchored
14
15 PDMS chip is robustly bonded on hydrogel matrix even when pulled by a tweezer. **c)** Physically
16
17 attached PDMS chip is easily debonded from hydrogel matrix. **d)** Chemically anchored PDMS
18
19 chip doesn't debond from hydrogel matrix even under high stretch (up to 3 times) due to robust
20
21 adhesion between adhesion layers. **e)** The calculated $G/\mu L$ from the finite-element model is plotted
22
23 as functions of λ and S/L . The typical values of interfacial toughness between chips and hydrogels
24
25 with and without silanized interfaces are also given for comparison (1000 J/m^2 and 20 J/m^2
26
27 respectively). **f)** A sheet of hydrogel (thickness $\sim 1.5 \text{ mm}$) with multiple patterned chips can
28
29 conformably attach to different regions of human body and survive deformation due to body
30
31 movements. **g)** A hydrogel electronic device that encapsulates an array of LED lights connected
32
33 by stretchable silanized titanium wire. The device is transparent, and robust under multiple cycles
34
35 of high stretch.
36
37
38
39
40
41
42
43
44
45
46
47
48
49
50
51
52
53
54
55
56
57
58
59
60
61
62
63
64
65

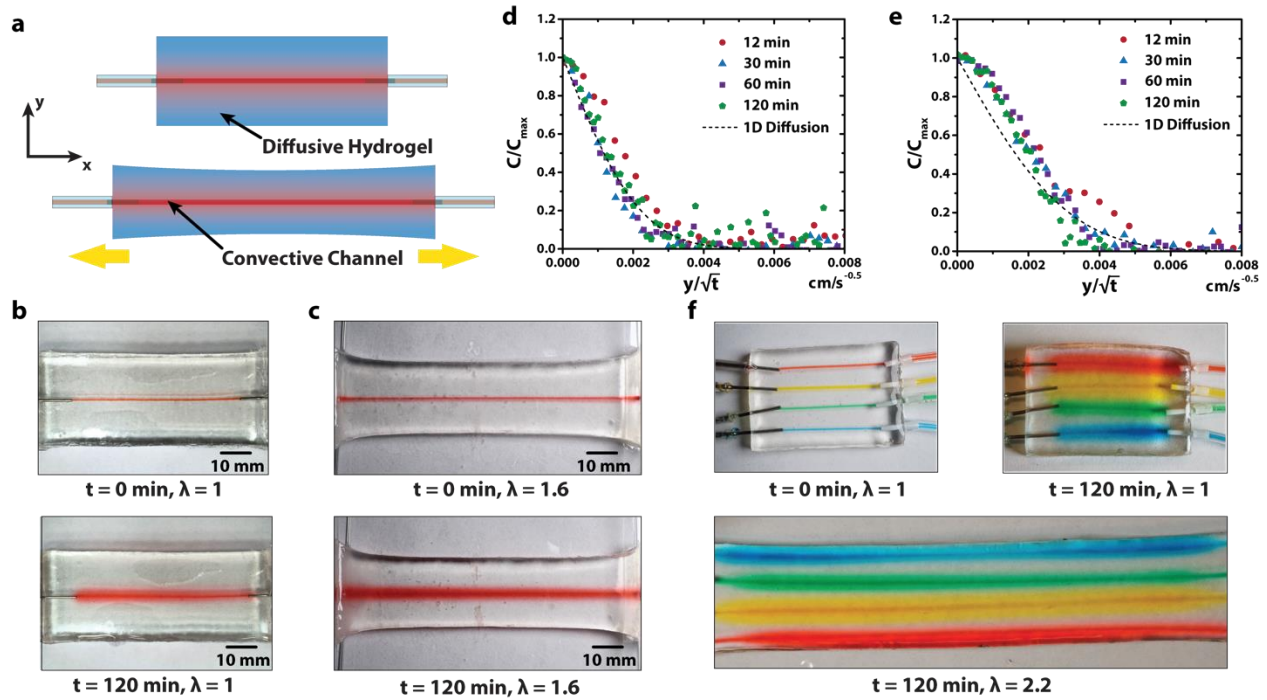


Figure 4. Integration of drug-delivery channels in tough hydrogel matrix. a) Schematic illustration of diffusion of drug solution inside hydrogel from the drug-delivery channel. b) Experimental snapshots of drug diffusion in the undeformed hydrogel. c) Experimental snapshots of drug diffusion in the deformed hydrogel. d) Normalized one-dimensional diffusion of mock drug inside undeformed hydrogel channel. e) Normalized one-dimensional diffusion of mock drug inside deformed ($\lambda = 1.6$) hydrogel channel. f) Experimental snapshots of the diffusion of multiple mock drugs in a hydrogel matrix under high stretches.

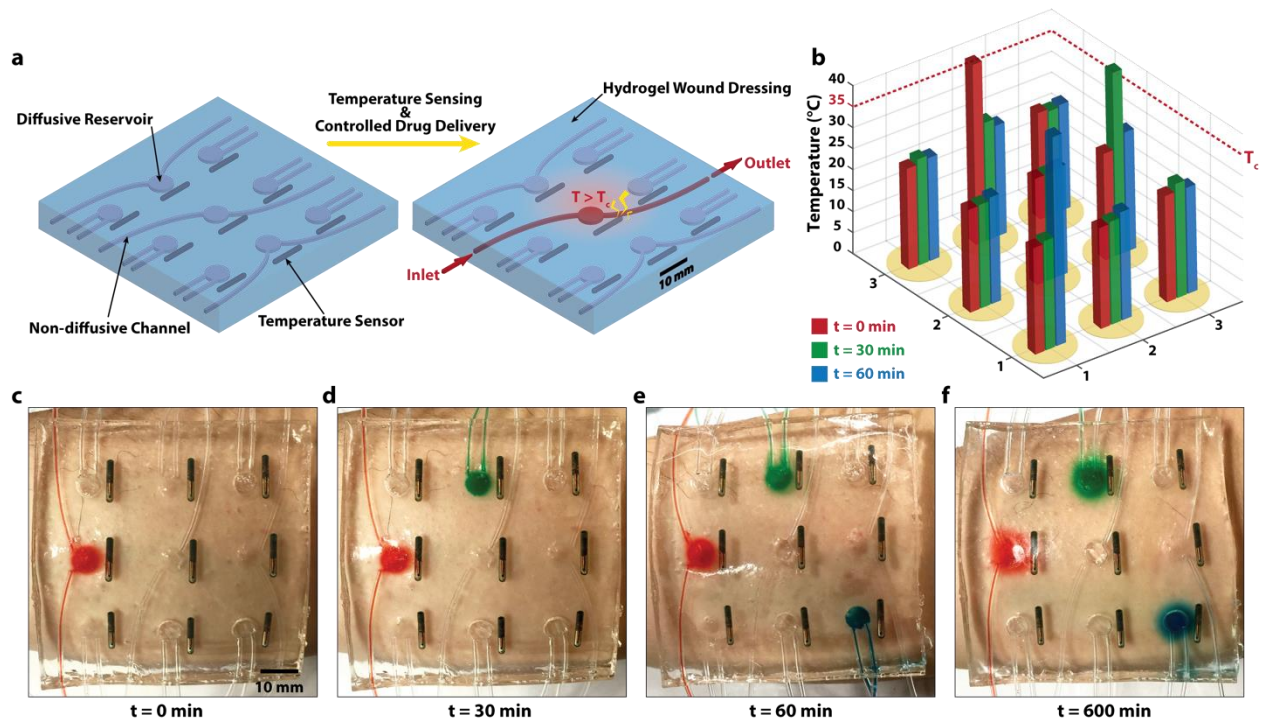


Figure 5. A smart wound dressing based on stretchable and biocompatible hydrogel device

a) The temperature sensors are patterned into a 3 by 3 matrix with a drug-delivery reservoir next to each of them. The smart wound dressing can give programmable and sustained deliveries of different drugs at various locations over human skin according to the temperatures measured at those locations. **b)** The temperatures at different locations on the skin are measured via wireless temperature sensor over time. **c-f)** When the temperature at a location goes above a certain level (e.g., $T_c = 35\text{ }^\circ\text{C}$), a mock drugs is injected through non-diffusive channels into the corresponding reservoir to diffuse out over time. Sustained releases of various drugs are achieved at different locations according to the temperatures measured at different times.

Reference

- [1] D. J. Beebe, J. S. Moore, J. M. Bauer, Q. Yu, R. H. Liu, C. Devadoss, B. H. Jo, *Nature* 2000, 404, 588.
- [2] L. Dong, A. K. Agarwal, D. J. Beebe, H. R. Jiang, *Nature* 2006, 442, 551.
- [3] J. D. Debord, S. Eustis, S. B. Debord, M. T. Lofye, L. A. Lyon, *Advanced Materials* 2002, 14, 658.
- [4] Y. Iwayama, J. Yamanaka, Y. Takiguchi, M. Takasaka, K. Ito, T. Shinohara, T. Sawada, M. Yonese, *Langmuir* 2003, 19, 977.
- [5] A. Sidorenko, T. Krupenkin, A. Taylor, P. Fratzl, J. Aizenberg, *Science* 2007, 315, 487.
- [6] J. Kim, J. A. Hanna, M. Byun, C. D. Santangelo, R. C. Hayward, *Science* 2012, 335, 1201.
- [7] S. Maeda, Y. Hara, T. Sakai, R. Yoshida, S. Hashimoto, *Advanced Materials* 2007, 19, 3480.
- [8] D. Morales, E. Palleau, M. D. Dickey, O. D. Velev, *Soft matter* 2014, 10, 1337.
- [9] E. Palleau, D. Morales, M. D. Dickey, O. D. Velev, *Nature communications* 2013, 4.
- [10] J.-W. Jeong, G. Shin, S. I. Park, K. J. Yu, L. Xu, J. A. Rogers, *Neuron* 2015, 86, 175.
- [11] J. A. Rogers, T. Someya, Y. Huang, *Science* 2010, 327, 1603.
- [12] S. Bauer, S. Bauer - Gogonea, I. Graz, M. Kaltenbrunner, C. Keplinger, R. Schwödiauer, *Advanced Materials* 2014, 26, 149.
- [13] M. L. Hammock, A. Chortos, B. C. K. Tee, J. B. H. Tok, Z. Bao, *Advanced Materials* 2013, 25, 5997.
- [14] N. Lu, *The Bridge on Frontiers of Engineering* 2013, 43, 31.
- [15] L. Pan, G. Yu, D. Zhai, H. R. Lee, W. Zhao, N. Liu, H. Wang, B. C.-K. Tee, Y. Shi, Y. Cui, *Proceedings of the National Academy of Sciences* 2012, 109, 9287.
- [16] C. Yu, Z. Duan, P. Yuan, Y. Li, Y. Su, X. Zhang, Y. Pan, L. L. Dai, R. G. Nuzzo, Y. Huang, *Advanced Materials* 2013, 25, 1541.
- [17] H. Warren, M. in het Panhuis, *Synthetic Metals* 2015, 206, 61.
- [18] J. P. Gong, Y. Katsuyama, T. Kurokawa, Y. Osada, *Advanced Materials* 2003, 15, 1155.
- [19] J.-Y. Sun, X. Zhao, W. R. K. Illeperuma, O. Chaudhuri, K. H. Oh, D. J. Mooney, J. J. Vlassak, Z. Suo, *Nature* 2012, 489, 133.
- [20] T. L. Sun, T. Kurokawa, S. Kuroda, A. B. Ihsan, T. Akasaki, K. Sato, M. A. Haque, T. Nakajima, J. P. Gong, *Nat Mater* 2013, 12, 932.
- [21] L. Stevens, P. Calvert, G. G. Wallace, *Soft Matter* 2013, 9, 3009.
- [22] H. Warren, R. D. Gately, P. O'Brien, R. Gorkin, *Journal of Polymer Science Part B: Polymer Physics* 2014, 52, 864.
- [23] J. P. Gong, *Soft Matter* 2010, 6, 2583.
- [24] X. Zhao, *Soft Matter* 2014, 10, 672.
- [25] T. Zhang, S. Lin, H. Yuk, X. Zhao, *Extreme Mechanics Letters* 2015, 4, 1.
- [26] J.-Y. Sun, X. Zhao, W. R. Illeperuma, O. Chaudhuri, K. H. Oh, D. J. Mooney, J. J. Vlassak, Z. Suo, *Nature* 2012, 489, 133.
- [27] S. Hong, D. Sycks, H. F. Chan, S. Lin, G. P. Lopez, F. Guilak, K. W. Leong, X. Zhao, *Advanced Materials* 2015, 27, 4035.
- [28] H. Yuk, T. Zhang, S. Lin, G. A. Parada, X. Zhao, *In submission* 2015.
- [29] K. Y. Lee, D. J. Mooney, *Chemical Reviews* 2001, 101, 1869.

- 1
2
3
4
5
6
7
8
9
10
11
12
13
14
15
16
17
18
19
20
21
22
23
24
25
26
27
28
29
30
31
32
33
34
35
36
37
38
39
40
41
42
43
44
45
46
47
48
49
50
51
52
53
54
55
56
57
58
59
60
61
62
63
64
65
- [30] M. C. Darnell, J.-Y. Sun, M. Mehta, C. Johnson, P. R. Arany, Z. Suo, D. J. Mooney, *Biomaterials* 2013, 34, 8042.
 - [31] C. Fan, L. Liao, C. Zhang, L. Liu, *Journal of Materials Chemistry B* 2013, 1, 4251.
 - [32] C. Lv, H. Yu, H. Jiang, *Extreme Mechanics Letters* 2014, 1, 29.
 - [33] J. He, R. G. Nuzzo, J. Rogers, *Proceedings of the IEEE* 2015, 103, 619.
 - [34] D.-H. Kim, J.-H. Ahn, W. M. Choi, H.-S. Kim, T.-H. Kim, J. Song, Y. Y. Huang, Z. Liu, C. Lu, J. A. Rogers, *Science* 2008, 320, 507.
 - [35] J.-H. Ahn, J. H. Je, *Journal of Physics D: Applied Physics* 2012, 45, 103001.
 - [36] K.-I. Jang, H. U. Chung, S. Xu, C. H. Lee, H. Luan, J. Jeong, H. Cheng, G.-T. Kim, S. Y. Han, J. W. Lee, J. Kim, M. Cho, F. Miao, Y. Yang, H. N. Jung, M. Flavin, H. Liu, G. W. Kong, K. J. Yu, S. I. Rhee, J. Chung, B. Kim, J. W. Kwak, M. H. Yun, J. Y. Kim, Y. M. Song, U. Paik, Y. Zhang, Y. Huang, J. A. Rogers, *Nat Commun* 2015, 6.
 - [37] C. Keplinger, J.-Y. Sun, C. C. Foo, P. Rothemund, G. M. Whitesides, Z. Suo, *Science* 2013, 341, 984.
 - [38] Q. Wang, L. Zhang, X. Zhao, *Physical review letters* 2011, 106, 118301.
 - [39] C. Cha, E. Antoniadou, M. Lee, J. H. Jeong, W. W. Ahmed, T. A. Saif, S. A. Boppart, H. Kong, *Angewandte Chemie International Edition* 2013, 52, 6949.
 - [40] N. Lu, J. Yoon, Z. Suo, *International Journal of Materials Research* 2007, 98, 717.
 - [41] N. A. Peppas, J. Z. Hilt, A. Khademhosseini, R. Langer, *ADVANCED MATERIALS-DEERFIELD BEACH THEN WEINHEIM-* 2006, 18, 1345.
 - [42] K. Y. Lee, D. J. Mooney, *Chemical reviews* 2001, 101, 1869.
 - [43] J. Y. Sun, X. H. Zhao, W. R. K. Illeperuma, O. Chaudhuri, K. H. Oh, D. J. Mooney, J. J. Vlassak, Z. G. Suo, *Nature* 2012, 489, 133.
 - [44] V. Dugas, Y. Chevalier, *Journal of colloid and interface science* 2003, 264, 354.
 - [45] W. Yoshida, R. P. Castro, J.-D. Jou, Y. Cohen, *Langmuir : the ACS journal of surfaces and colloids* 2001, 17, 5882.
 - [46] B. V. Muir, D. Myung, W. Knoll, C. W. Frank, *ACS Appl Mater Interfaces* 2014, 6, 958.
 - [47] D. C. Duffy, J. C. McDonald, O. J. Schueller, G. M. Whitesides, *Analytical chemistry* 1998, 70, 4974.
 - [48] A. P. Golden, J. Tien, *Lab on a Chip* 2007, 7, 720.

1
2
3
4 **Supplementary Materials for**

5
6
7 **Stretchable, Robust and Biocompatible Hydrogel Electronics and Devices**

8
9 *Shaoting Lin^{1a}, Hyunwoo Yuk^{1a}, Teng Zhang^{1a}, Hyunwoo Koo^{1,2}, Cunjiang Yu³, and Xuanhe Zhao^{1,4*}*

10
11
12 *¹ Soft Active Materials Laboratory, Department of Mechanical Engineering, Massachusetts Institute of*
13
14 *Technology, Cambridge, MA 02139, USA; ² Samsung Display, Asan-City, Chungcheongnam-Do, Korea*

15
16
17 *³ Department of Mechanical Engineering, University of Houston, Houston, TX 77204, USA; ⁴ Department of*
18
19 *Civil and Environmental Engineering, Massachusetts Institute of Technology, Cambridge, MA 02139, USA*

20
21 *^a These authors contribute equally to the current work.*

22
23 ** To whom correspondence should be addressed. Email: zhaox@mit.edu*

24
25
26
27
28 **This PDF file includes:**

29
30
31 Numerical Simulations

32
33
34 Supplementary Figure 1 to 9

35
36
37 Captions for Supplementary Videos S1 to S4

38
39
40
41
42
43 **Other Supplementary Materials for this manuscript includes the following:**

44
45
46 Supplementary Videos S1 to S4

47
48
49
50
51
52
53
54
55
56
57
58
59
60
61
62
63
64
65

Numerical Simulations

The numerical simulations of deformation of failure of hydrogel electronics and devices were performed with finite-element software, Abaqus/standard. Since the effect of water transportation is negligible during the time of hydrogel deformation, the hydrogel was modeled as an incompressible Neo-hookean material,

$$W = \mu/2(\lambda_1^2 + \lambda_2^2 + \lambda_3^2 - 3) \quad (S1)$$

where W is the strain energy density, μ the shear modulus and λ_i the i th principle stretch ($i=1,2,3$). Throughout the simulations, we took μ as 10 kPa to represent the typical elastic modulus of the hydrogels.

Numerical Simulation for hydrogel samples with Titanium wire encapsulated. Since the hydrogel strip with titanium wire encapsulated exhibited periodical wavy structures, we only simulated half of one period and employed symmetry boundary at the two sides of the edges. The hydrogel strip had a height of 50 mm, width of 6.4 mm and thickness as 3 mm. The wavy titanium wire followed the sinusoidal shape with a period length as 12.8 mm and amplitude as 3.3 mm. The cross section of the titanium was a cylinder with radius 0.1 mm. Titanium was modelled as a linear elastic material with Young's modulus of 100 GPa and Poisson's ratio of 0.3. The hydrogel was discretized with an 8-node linear brick, hybrid element (C3D8RH), and the titanium wire was modeled as a 2-node linear beam, hybrid element (B31H). A "Tie" constraint was applied to titanium wire and hydrogel to bond them together. A displacement loading was applied to the right edge of the whole structure including the hydrogel strip and titanium wire.

Numerical Simulation for hydrogel samples with hard islands bonded. As shown in **Fig. S6a**, we studied the structures of a hydrogel substrate with periodically patterned rigid islands and adopted a

1
2
3
4 two-dimensional plane strain-model to simulate one period of the structure only (**Fig. S6b**). The center-
5
6 to-center distance between two adjacent rigid islands was denoted as S . The hydrogel substrate had
7
8 a thickness of H , and the island had a width of L . The hydrogel was modeled with a 4-node bilinear plane
9
10 strain, hybrid element (CPE4RH). Symmetry boundary was applied to the left edge of the hydrogel. A
11
12 displacement loading along the x direction was applied to the right edge of the hydrogel substrate. The
13
14 surface of hydrogel beneath the rigid island was constrained.
15
16
17
18
19
20

21 **Calculation of energy release rate.** To calculate the energy release rate of the hydrogel substrate
22
23 with rigid island bonded, we released the bonded interface for a small distance, denoted as ΔL , and
24
25 performed the simulation with all rest conditions kept unchanged (**Fig. S7a-b**). We focused on the
26
27 symmetry crack mode, which corresponds a $\Delta L/2$ crack advancement at each edge of the interface
28
29 between island and hydrogel substrate. The total strain energy for structures with the perfectly bonded and
30
31 partially released interface were recorded as $U(L)$ and $U(L - \Delta L)$, respectively. Then, the energy
32
33 release rate for the interfacial crack propagation can be expressed as
34
35
36
37
38

$$39 \quad G = \frac{U(L) - U(L - \Delta L)}{\Delta L} \quad (S2)$$

40
41
42

43 To test the effect of the hydrogel thickness on the energy release rate, we first simulated the cases with S
44
45 = 20 mm, $L = 10$ mm, and H varying from 100 mm to 1 mm. The calculated energy release rates were
46
47 shown in **Fig. S7c**. It can be seen that the energy release rate gradually decreases with the decrease of H .
48
49 Therefore, we mainly focused on the analysis of very thick hydrogel (i.e., $H = 100$ mm) for a conservative
50
51 design. In order to examine the effect of the center distance of the two adjacent chips, we kept the width
52
53 of the chip unchanged (i.e., $L = 10$ mm) and varied S from 16 mm to 25 mm. The results are shown in the
54
55 main text (**Fig. 3e**).
56
57
58
59
60
61
62
63
64
65

1
2
3
4
5
6
7 **Table S1. Ingredients of McCormick food dyes as mock drugs**
8

9

	Ingradients
Red food dye	Water. Propylene Glycol, FD&C Yellow 5, FD&C Blue 1 and Propylparaben
Yellow food dye	Water. Propylene Glycol, FD&C Reds 40 AND 3, and Propylparaben
Green food dye	Water. Propylene Glycol, FD&C Yellow5, Propylparaben, and Red 40
Blue food dye	Water. Propylene Glycol, FD&C Blue 1 and Red 40, and Propylparaben

10
11
12
13
14
15
16
17
18
19
20
21
22
23
24
25
26
27
28
29
30
31
32
33
34
35
36
37
38
39
40
41
42
43
44
45
46
47
48
49
50
51
52
53
54
55
56
57
58
59
60
61
62
63
64
65

Supplementary Figures and Captions

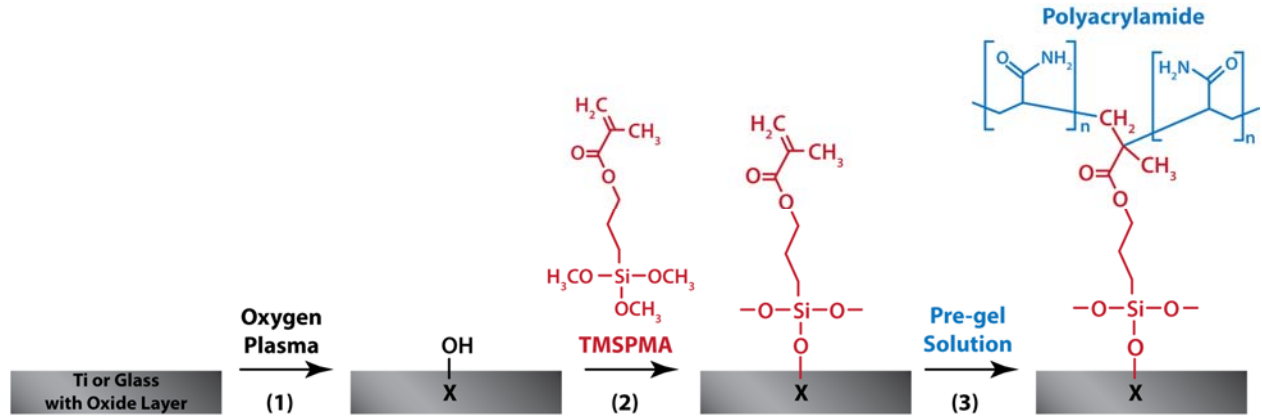


Figure S1. The titanium wire and glass slide were exposed to oxygen plasma to introduce hydroxyl-activated surface oxides on their surfaces. Functional silane TMSPPMA was then grafted onto the hydroxyl-activated surface through siloxane covalent chemistry. The long-chain polymer network of PAAm was then covalently crosslinked to the grafted silane.

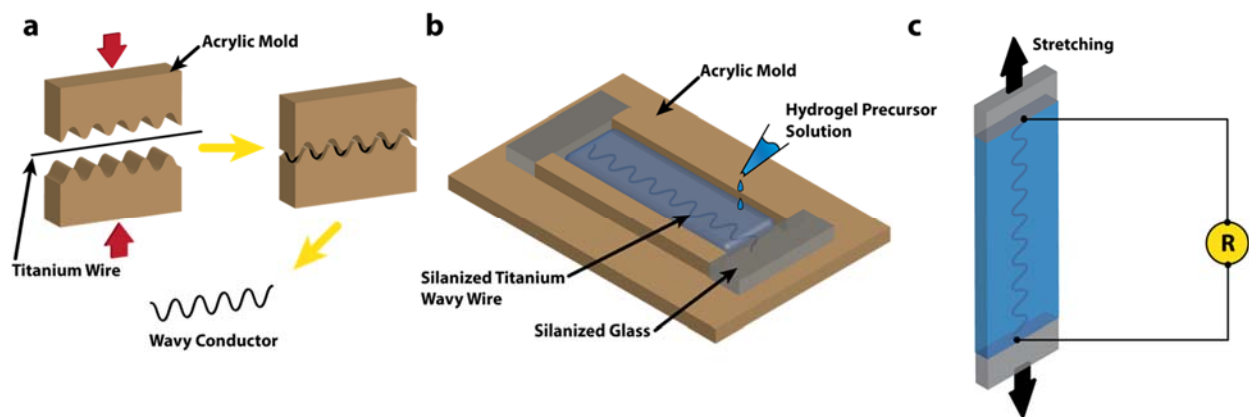


Figure S2. **a)** Wavy conductor was fabricated by pressing plastically deformable titanium wire in between acrylic molds with predetermined sinusoidal shapes. **b)** Fabrication of hydrogel sample with silanized titanium wire encapsulated. **c)** Schematic illustration of test set up for the measurement of both stretchability and resistance of hydrogel conductor.

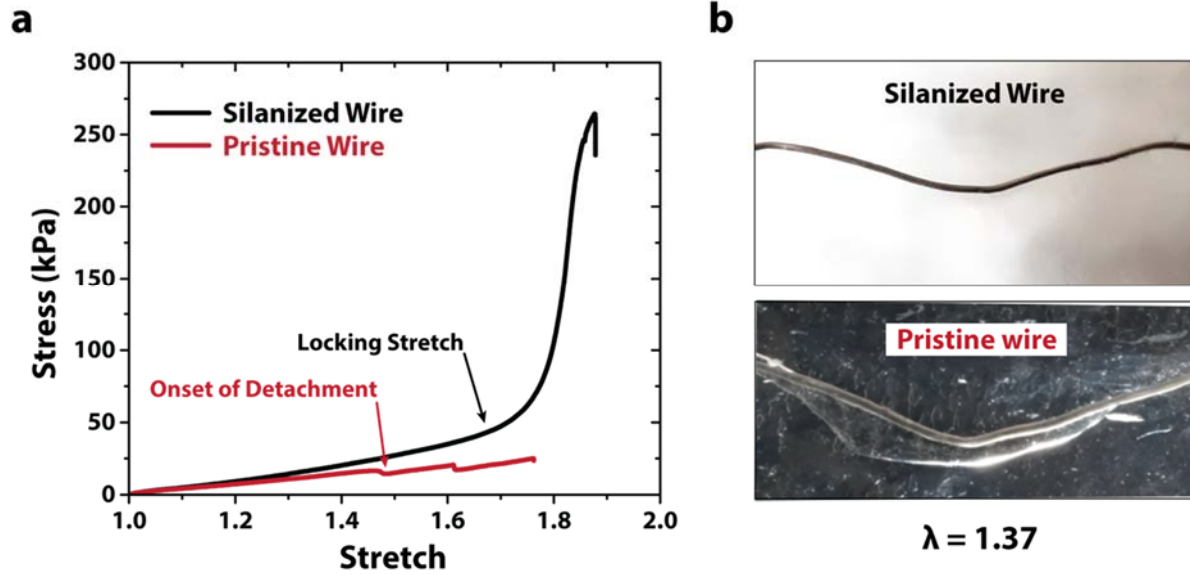


Figure S3. a) Comparison of stress-stretch curves of the sample encapsulated with silanized titanium wire and pristine titanium wire. Note that the dimension of titanium wire is $A/L = 0.46$. **b)** Comparison of the interfaces between silanized wire-hydrogel and pristine wire-hydrogel in stretched sample.

1
2
3
4
5
6
7
8
9
10
11
12
13
14
15
16
17
18
19
20
21
22
23
24
25
26
27
28
29
30
31
32
33
34
35
36
37
38
39
40
41
42
43
44
45
46
47
48
49
50
51
52
53
54
55
56
57
58
59
60
61
62
63
64
65

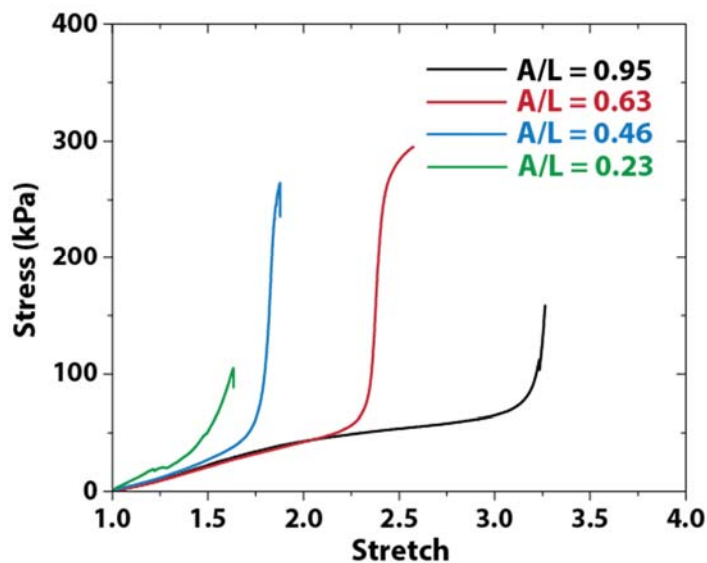
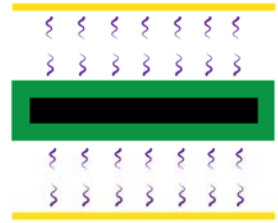
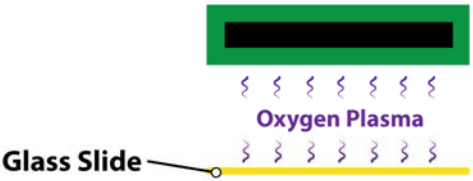


Figure S4. Stress strain curves of hydrogel conductors with silanized titanium wire of different dimensions. The sample is soft and compliant in small and moderate deformation. When the stretch reaches the locking stretch, the stress increases dramatically indicating that the titanium wire is nearly straightened.

1
2
3
4
5
6
7
8
9
10
11
12
13
14
15
16
17
18
19
20
21
22
23
24
25
26
27
28
29
30
31
32
33
34
35
36
37
38
39
40
41
42
43
44
45
46
47
48
49
50
51
52
53
54
55
56
57
58
59
60
61
62
63
64
65

Rigid Electric Component

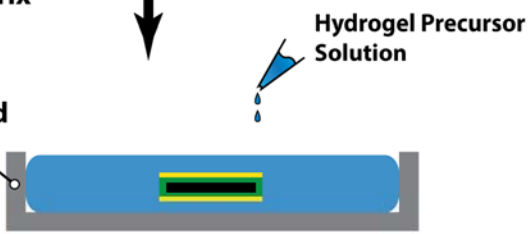
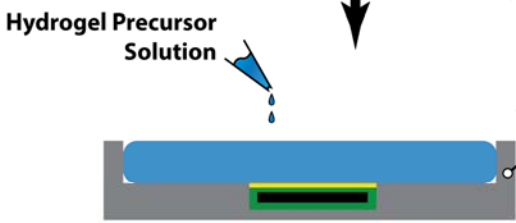
↓ **PDMS Coating**



↓ **Physical Contact (PDMS-Glass bonding)**



↓ **Glass Silanation (TMSPMA Solution) & Adhering on/into Hydrogel Matrix**



↓ **Hydrogel Curing**



I. PDMS Chip on Surface

II. PDMS Chip inside Matrix

1
2
3
4 **Figure S5.** Fabrication of PDMS islands onto/inside hydrogel matrix. Rigid electric components are
5 encapsulated by PDMS to protect them from wet hydrogel environment. PDMS chip and glass slide are
6 bonded by exposing both surface with oxygen plasma and physically contact them to form siloxane
7 covalent bond at the interface. PDMS chip with glass slide is adhered onto hydrogel matrix by using
8 acrylic mold. Notably, PDMS chip can be installed inside hydrogel matrix by putting it at the middle of
9 partially cured precursor solution.
10
11
12
13
14
15
16
17
18
19
20
21
22
23
24
25
26
27
28
29
30
31
32
33
34
35
36
37
38
39
40
41
42
43
44
45
46
47
48
49
50
51
52
53
54
55
56
57
58
59
60
61
62
63
64
65

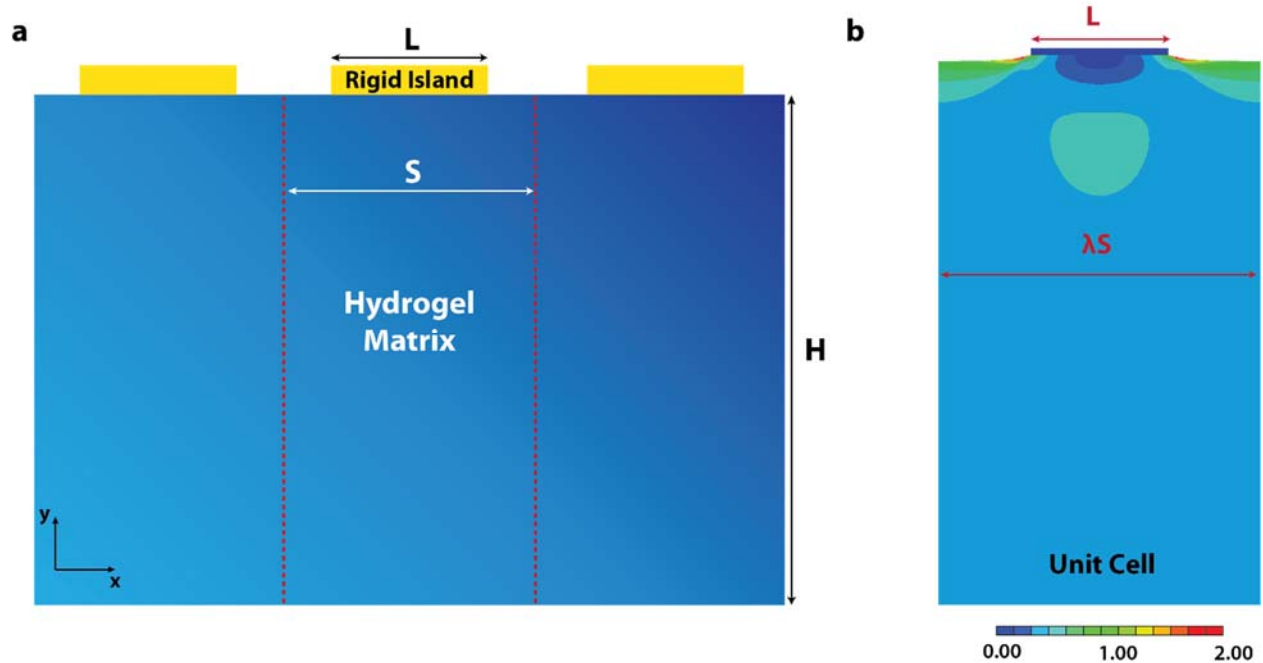


Figure S6. a) Schematic illustration of periodically patterned hard islands and adopted a two-dimensional plane strain model to simulate one period of the structure only. The center-to-center distance between two adjacent hard islands was denoted as S . The hydrogel substrate had a thickness of H , and the island had a width of L and height h . b) FEM simulation result for single unit cell under deformation.

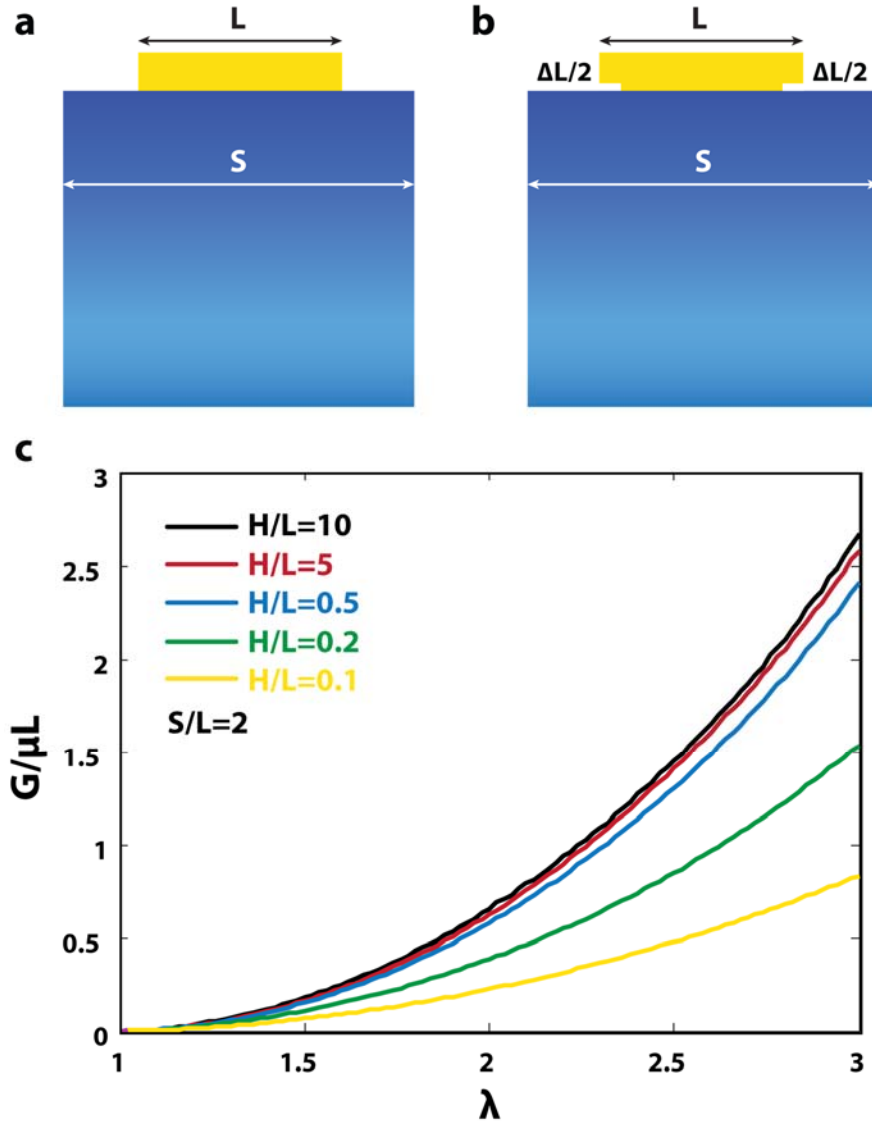


Figure S7. a-b) To calculate the energy release rate of the hydrogel substrate with hard island bonded, we artificially released the bonded interface for a small distance, denoted as ΔL , and performed the simulation with all rest conditions kept unchanged. **c)** The calculated the energy release rate curves for different H/L ratios. It can be seen that the energy release rate gradually decreases with the width H .

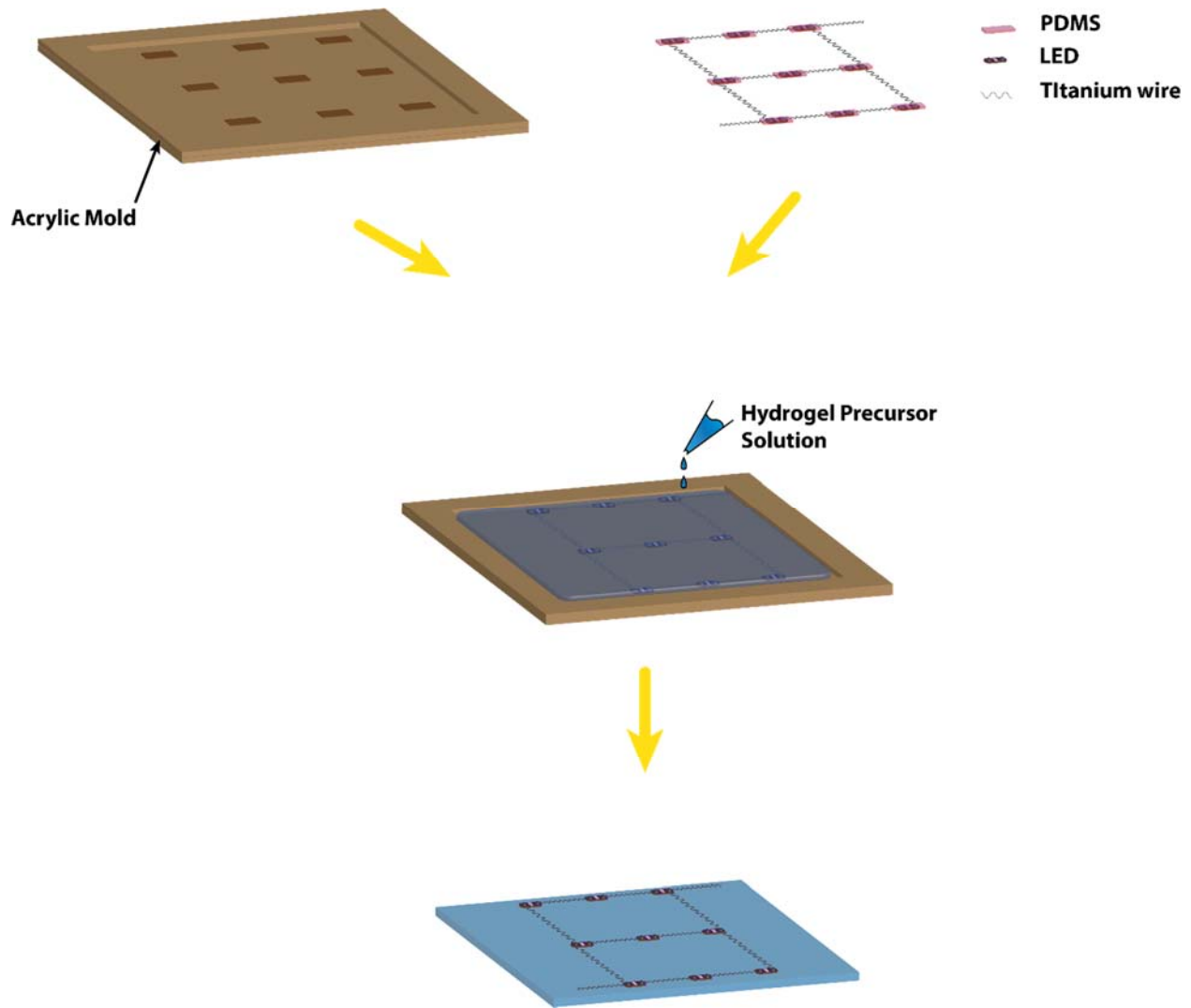


Figure S8. Fabrication of an array of LED lights connected by stretchable wires encapsulated in hydrogel matrix. Laser cutter was utilized to make the acrylic mold with 3 by 3 holes. Thereafter, an array of LED lights (encapsulated in PDMS) connected by sinusoid silanized titanium wire were placed in the mold with LED in the holes. To ensure the high adhesion between rigid components (LED lights) and hydrogel matrix, bonding procedure shown in **Fig. S5** was utilized. Precursor hydrogel solution was infused in the mold and cured in UV oven for 60 minutes with 8 W power and 254 nm wavelength.

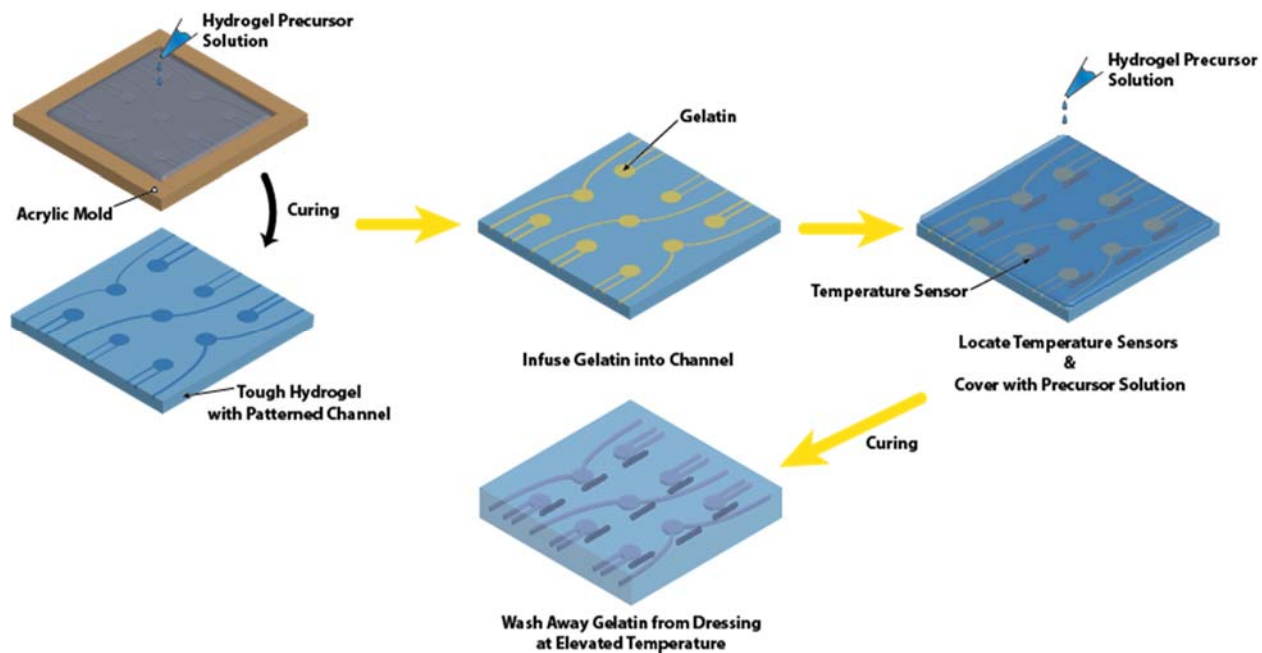


Figure S9. The one side of smart wound dressing is fabricated by curing hydrogel precursor solution onto acrylic mold with pattern of channels and reservoirs. After curing, patterned channels and reservoirs were infused by molten gelatin solution. The sample was kept inside refrigerator to solidify gelatin. Thereafter, temperature sensors were placed beside each reservoirs and top surface was covered by another layer of precursor solution. After curing top hydrogel layer, the infused gelatin was molten inside oven and then washed away using deionized water multiple times.

1
2
3
4
5
6
7
8
9
10
11
12
13
14
15
16
17
18
19
20
21
22
23
24
25
26
27
28
29
30
31
32
33
34
35
36
37
38
39
40
41
42
43
44
45
46
47
48
49
50
51
52
53
54
55
56
57
58
59
60
61
62
63
64
65

Captions for Supplementary Videos

Supplementary Video S1

A hydrogel conductor that contains a silanized titanium wire ($A/L=0.31$) being stretched to the theoretical limit of stretch $\lambda_{\max} \approx 1.58$. The hydrogel conductor maintains high conductivity during the stretching process, indicated by LED lights connected to a DC battery via the hydrogel conductor.

Supplementary Video S2

PDMS island is strongly bonded on the surface of tough hydrogel and can survive pulling by tweezers.

Supplementary Video S3

Array of LEDs encapsulated by PDMS are installed inside tough hydrogel matrix, and interconnected by wavy conductors for electric connection. The circuit can retain its functionality under large cyclic deformation due to strong adhesion between functional electric components and hydrogel matrix.

Supplementary Video S4

Smart wound dressing selectively delivers multiple dyes from diffusive hydrogel reservoirs based on temperature signals.

Video S1

[Click here to download Supporting Information: Video S1.mp4](#)

Video S2

[Click here to download Supporting Information: Video S2.mp4](#)

Video S3

[Click here to download Supporting Information: Video S3.mp4](#)

Video S4

[Click here to download Supporting Information: Video S4.mp4](#)